Bioprinting 3-Dimensional Skeletal Muscle Tissue Models Using Decellularized Extracellular Matrix

Zeid Yousef Nawas

A thesis

submitted in partial fulfillment of the

requirements for the degree of

Master of Science in Bioengineering

University of Washington

2017

Committee:

Deok-Ho Kim

Kelly Stevens

Program Authorized to Offer Degree:

Bioengineering

University of Washington

Abstract

Bioprinting 3-Dimensional Skeletal Muscle Tissue Models
Using Decellularized Extracellular Matrix

Zeid Yousef Nawas

Chair of the Supervisory Committee:

Dr. Deok-Ho Kim

Bioengineering

Developing biologically relevant models of human tissues and organs is an important enabling step for many applications within biological research and medicine. A specific application that physiologically relevant tissue models can be implemented in is drug discovery. In this study, we represent a platform and methodology of generating 3D humanized physiologically relevant skeletal muscle tissues that recapitulate aspects of the native cellular microenvironment found in the native skeletal muscles for the development of a reproducible and high-throughput drug-screening model. This is achieved by utilizing a 3D bioprinting platform in conjugation with

human myoblasts-laden decellularized extracellular matrix (dECM) bioinks to form skeletal muscle tissue constructs. Structures that feature a skeletal muscle tissue that is anchored on both sides by rigid structures are printed. The rigid anchor structures would induce passive tension along the skeletal muscle tissue, which influences cellular alignment and orientation along the anchors' axis of tension. The results described in this study demonstrate our ability to generate human 3D skeletal muscle tissues in a rapid, high-throughput, and reproducible manner, which can be implemented as a predictive drug screening tool for determining the effects that a novel drug may have in the human body.

TABLE OF CONTENTS

LIST OF FIGURES

LIST OF TABLES

ACKNOWLEDGEMENTS

I would like to extend my deep gratitude to Dr. Deok-Ho Kim, my advisor in both my undergraduate and graduate career. Dr. Kim is extremely passionate about his research, and his enthusiasm and thirst for exploration and innovation are obvious and infectious. Dr. Kim has always pushed me to achieve the highest quality research, and to hold myself to the highest standards of work and professionalism. I greatly appreciate the opportunity he has given me to pursue research in his laboratory.

I would also like to thank Dr. Kelly Stevens for the assistance and time she offered as a committee member for my thesis.

Jonathan Tsui, a PhD student in the Kim lab, provided me with valuable guidance as my direct mentor in Dr. Kim's lab through both my undergraduate and graduate studies. He consistently provided support and fresh perspective to the challenges I faced, and I consider him one of the most capable scientists and researchers I have had the pleasure of working with.

I would also like to thank Dr. Alec Smith, who provided me tremendous support in technical and organizational aspects of my project. Whenever I ran into setbacks, he was always willing to help me navigate an effective plan of action.

Joseph Long, a visiting researcher, helped me establish the project from the initial phases. He was always willing to work beside me, provide me with advice and technical support.

Som Chavanachat an undergraduate researcher at the Kim lab has provided me with a lot of help in obtaining many of the biological end points for this project.

Chapter 1. INTRODUCTION

1.1 MOTIVATION

In order for drugs to go from discovery to market, they must go through the drug approval process, which includes laboratory, pre-clinical, and clinical test phases. The drug discovery process takes about 10-15 years and $1.7 billion per drug [1], [2]. In the initial phases of this process, approximately 10,000 compounds are discovered and identified as possible effective drugs. Of those, 250 compounds reach the pre-clinical phases and only 5 compounds pass on to the clinical trials phase. However, on average, only 1 of the drugs that do actually reach clinical trials is approved (**Figure 1**).

What is important to note is the fact that, out of every 5 compounds that's do make it into clinical trials, only 1 is approved, resulting in an 80% failure rate, highlighting the fact that the pre-clinical predictability was poor. Since they are poor tests, this means there's a possibility the wrong compounds are screened out. Some of the 250 that are screened out might possibly be effective and advantageous when administered to a patient, while others that do pass are in fact toxic and might harm the patients. This ultimately results in huge amounts of money and resources lost that can be used for the development of alternative compounds, which are actually effective [3].

There are two currently employed methods of screening out compounds in the pre-clinical phases: animal models and 2D cell cultures. In the animal models approach, the compound of interest is administered to an animal and then possible side effects are observed [4], [5]. Those results and conclusions are then translated to humans. In other words, if a side effect arises in the animal due to the compound administered, it is concluded that that same effect would be observed

in human patients. However, this method is an ineffective and inefficient way for screening drugs [6]–[8]. Animals cannot fully recapitulate the clinical, physiological, and biochemical characteristics found in humans, thus results and conclusions drawn from these models often do not translate to humans. Additionally, another major limitation of this method is the fact that it is inherently a low throughput screening system.

As for using 2D culture assays, the compound of interest is introduced into the culture and changes in structure and function of the cells are observed. The results and conclusions of these systems are then used to determine possible side effects or effectiveness of the drug when administered to patients. However, such systems are not capable of recapitulating the intrinsic complexity of the 3D native human tissue and fail to mimic the *in-vivo* niche [5]. Additionally, 2D culture assays are often limited by their inability to directly measure muscle function and phenotype.

In-vitro models that feature patient-derived cells that are high throughput, fully defined, and biomimetic present exciting new technologies to augment the current *in-vivo* studies. Such models would enable investigators the collection of more predictive data in terms of the effect of new chemical compounds on human tissues. It is estimated that if the number of approved compounds is increased from 1 to just 2, approximately 6 years and $400 million dollars can be saved per drug. These resources can then be allocated towards other drugs that might benefit patients. In this regard, a combination of *in-vivo* testing and *in-vitro* screening using engineered human muscle models will likely lead to more stringent control of compounds progressing to clinical trial, and thereby ensure better translation of benchtop results to human patients, as well as saving money and resources that can be allocated towards the discovery and development of effective drugs.

One specific tissue that currently has poor models available that are utilized in drug-screening are skeletal muscle tissues, and there is a dire need for a more predictive assay that can improve the drug discovery process. Skeletal muscle is an attractive candidate for attempts to create in a laboratory setting because it is a tissue that responds to mechanical cues and as engineers, understanding mechanical cues is central to the field. Additionally, skeletal muscle tissues are relatively simple in composition, architecture, and development. Thus, it provides an opportunity to generate these tissues for their use in drug screening and potentially lead to the elimination of the inefficiencies and ineffectiveness involved in the current drug discovery process.

1.2 BACKGROUND

1.2.1 *Skeletal Muscle Physiology and Composition*

Skeletal muscle tissues are primarily made up of highly oriented and aligned contractile fibers that bring about the controlled contraction of the tissue and enable skeletal manipulation (**Figure 2**) [9]. Another major component of skeletal muscle tissues is the extracellular matrix (ECM), which makes up the perimysium, endomysium, and epimysium [10].

The ECM is the underlying support system or mesh of tissues. It is crucial that cells are embedded in this framework, where they are supported, having contact with neighboring cells and the extracellular matrix in order to function [11]–[14]. The matrix gives strength and flexibility to the tissue, while serving as a selective filter to control the flow of materials between cells [15], [16]. It has been shown that the ECM provides the cells with crucial mechanical and chemical cues provided by the different proteins, growth factors and other molecules found in its composition. These cues can improve maturation, survival and long-term function of the cells [17]. One important thing to note is the fact the ECM is tissue specific, in that the ECM of each tissue is

unique in terms of composition and topology, which is generated through dynamic and reciprocal interactions between the cells and microenvironment [18].

1.2.2 *Current Approaches for Generating Biomimetic Skeletal Muscle Models*

1.2.2.1 Generating Biomimetic 2D Skeletal Muscle Models

Engineered skeletal muscle comprising of immature cells are incapable of accurately recapitulating and reconstituting the phenotype and function of the *in-vivo* adult tissue. Thus, in order to successfully engineer skeletal muscle models, methodologies that recapitulate embryonic development and are able to promote maturation of cultured skeletal muscle myoblasts so that they are biomimetic of the native tissues need to be developed.

Culture Period

It has been shown that the regulation of tissue development is time-dependent, which is representative of the developmental process of the native tissue, which takes months or even years to attain an adult phenotype [19]. Thus, increasing the length of time in culture improves maturation state and function of the myoblasts *in-vitro*. While this long-term culture methodology is a well-established approach to enhance cellular maturation, reliance on such extended culturing timelines limits the efficiency of this method of generating tissues for widespread pre-clinical and clinical applications. Thus, given the obvious issues with throughput and long culturing times before a specific cell population would be suitably matured for use, efforts are made to pursue alternative methods of promoting maturation in *in-vitro* muscle cells.

Anisotropy

Skeletal muscles are highly aligned structures *in-vivo*, which facilitates their biological function. Previous studies have been able to show that cultures on nanoscale topographies show enhanced cellular alignment, maturation, and function over cells on unpatterned plastic [20]. Surface patterning has been utilized to promote the uniaxial alignment of cultured myogenic cells, where such surfaces have been shown to promote myotube maturation, featuring greater levels of sarcomeric development [21]. Similarly, microcontact printing has proven effective for patterning skeletal muscle culture surfaces that promote alignment and rates of fusion for differentiating myotubes [22]. While using these topological physical cues to guide and enhance the development of skeletal muscle cells, the 3-dimensional properties and chemical cues present in the native *in-vivo* tissues are not fully recapitulated.

Substrate Elasticity

Skeletal muscle myotubes are highly influenced by the mechanical properties of the surrounding tissue [23], [24]. A major issue for the long-term culturing of the skeletal muscle tissues is the rigidity of the culture plate surface. Previously published studies have been able to show substrate stiffness that matches that of the native tissue will produce optimal skeletal muscle maturation [25], [26]. However, again, this specific methodology is not capable of recapitulating the 3-dimensional complexity of the native tissue.

1.2.2.2 Generating Biomimetic 3D Skeletal Muscle Models

2D *in-vitro* culture environments provide a fundamentally alien setting for cultured cells. In contrast, 3D tissue constructs enable binding of the cell to ECM proteins over the entire cell

surface, resulting in a more biomimetic microenvironment for the embedded cells [5]. Additionally, the flexibility of the 3D matrix enhances cellular maturation, and application of uniaxial anchoring points can lead to the development of 3D cellular anisotropy because cells reorganize along the axis of tension within the construct.

There have been many previously published works were the generation of a more biomimetic skeletal muscle tissue structures was attempted. Vanderburgh *et al*. describe a method of generating 3D skeletal muscle tissue constructs composed of a collagen and Matrigel material embedded with C2C12s, an immortalized mouse cell line [27]. This tissue was anchored down on both sides and cultured. This group was able to show that with this method, they generated a rodent skeletal muscle tissue model that featured highly oriented aligned cells, which is in keeping with what is observed in human *in-vivo* skeletal muscle tissues. However, the group utilized a murine cell line and non-tissue specific biomaterial to create these tissues. Which means the crucial cues provided by the native ECM are not fully recapitulated in their proposed tissue model. In addition, the process of generating these skeletal muscle tissues is very labor intensive and involves mostly manual work. Inherently, manual work and human involvement in the making of these tissues is prone to introducing human error and variations. Thus, the degree of consistency and reproducibility of generating these tissues is questionable.

1.2.2.3 3D Bioprinting

Recent advances in bioprinting technology provide further options for the synthesis of complex 3D muscle tissues with a greater degree of reproducibility and uniformity for application in high-throughput drug screens and disease-modeling assays [28]. Mozetic *et al*. describe an approach of generating biomimetic 3D tissue models, where 3D bioprinting was utilized to generate rodent

skeletal muscle tissue structures [29]. They specifically utilized C2C12-laden Pluronic and alginate biomaterial, which was deposited in a square-wave fashion. The group was able to show that they achieve cellular alignment within the printed constructs and by utilizing an automated bioprinting system, it is likely that this presented a rapid, consistent and reproducible approach for tissue engineering. However, this study ultimately utilized a murine cell line and non-tissue specific biomaterial to generate these skeletal muscle tissues, which suggest that the resultant tissue structures cannot recapitulate and represent the native human *in-vivo* skeletal muscle tissues.

1.3 SUMMARY

In summary, currently employed pre-clinical drug screening assays, such as animal models and 2D cell cultures are ineffective and inefficient methods of determining possible effects of a compound on the human body. Several advances have been made in the field of tissue engineering that enable investigators to improve phenotype, function, and maturation of 2D *in-vitro* skeletal muscle monolayers and single cell models to be used to screen drugs. However, such models are limited by their inability to recapitulate the complexity of the 3D native skeletal muscle tissues in the human body. In response to the limitations present in currently employed drug screening models and tissue engineering techniques, we propose the development of an *in-vitro* human 3-dimensional physiologically relevant model that recapitulates aspects of the native cellular microenvironment found in the native skeletal muscles for the development of a reproducible and high-throughput drug-screening model in a rapid manner.

1.4 THESIS OUTLINE

In this thesis, we propose the development of an *in-vitro* human 3-dimensional physiologically relevant model that recapitulates aspects of the native cellular microenvironment found in the native skeletal muscles. This will be achieved by fully bioprinting biomimetic human skeletal muscle tissues, which feature a tissue-specific microenvironment and highly-aligned and oriented cellular structures. We will optimize the materials, printing process and design utilized in generating these tissue models, then investigate the resultant live tissues' structural and functional characteristics.

In Chapter 2, we demonstrate the ability to generate 3D bioprinting physiologically relevant human skeletal muscle tissue models in a rapid, high throughput and reproducible manner.

In Chapter 3, we demonstrate the cellular viability, cellular alignment, maturity and functionality induced by decellularized extracellular matrix bioinks and uniaxial anchor pair systems.

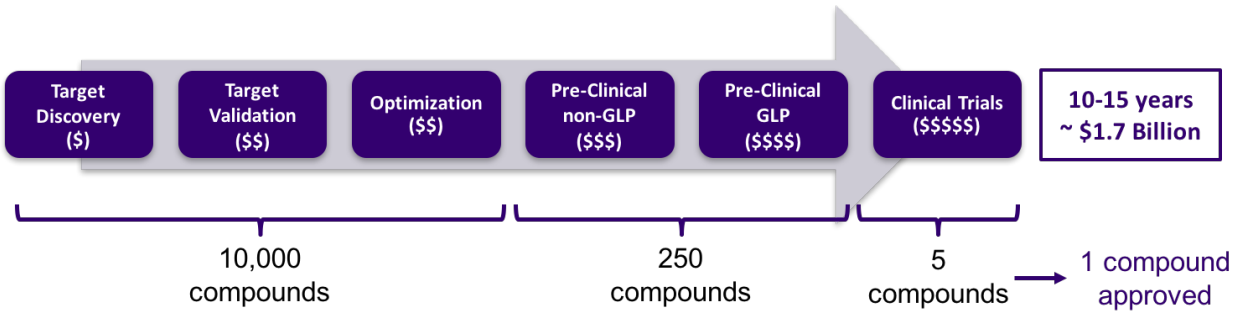

Figure 1: Schematic of drug discovery process

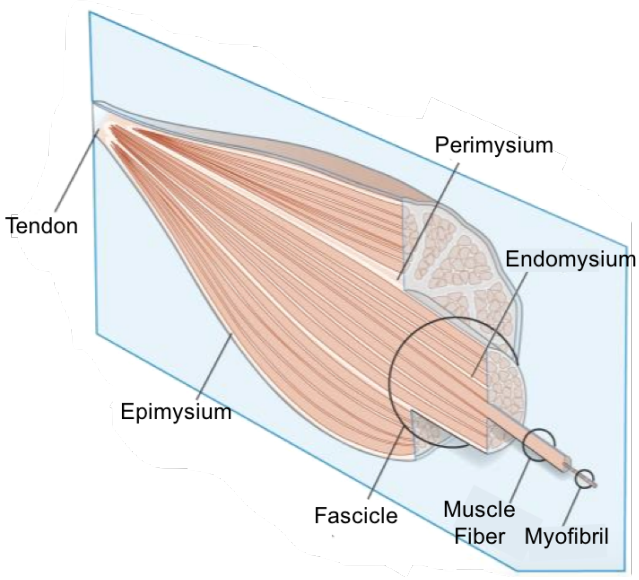

Figure 2: Schematic diagram of the gross organization of muscle tissue and muscle ECM organization. Gillies, *et al*. Muscle Nerve 2011

Chapter 2. Optimize Materials, Platform, And Design for Bioprinting 3D Skeletal Muscle Tissue

2.1 INTRODUCTION

One of the most promising and advanced fabrication methods that have emerged recently is 3D bioprinting. It is an additive manufacturing fabrication technique with which cell-laden biomaterials are utilized to build functioning tissues in a layer-by-layer fashion [30]. It is made up the extruders, typically a syringe and needle–which is where the cell-laden biomaterials (bioink) are held, motion controllers–which moves the extruders within 3-axes, and the computer-generated code–which controls the entire system including the bioink deposition.

My senior capstone project was focused on generating a bioprinting platform, which the Kim lab can use for generating 3D live tissue. In order to do so, retrofitting a well-established, optimized, and affordable normal 3D-printer (MakerBot) was attempted, where it would be converted into a bioprinter capable of depositing cell-laden bioinks. The MakerBot plastic extrusion mechanism was replaced with a pressure-driven extrusion mechanism, which featured a pneumatic valve control and a 60 mL bioink reservoir; however, all of the MakerBot's original optimized motion systems were unchanged. We demonstrated the successful retrofitting of the MakerBot and converting it into a functioning bioprinter with which bioinks can be deposited in a layer-by-layer manner.

Soon after, a 3D bioprinter called the BioBot became commercially available, which featured many similar aspects as the retrofitted MakerBot bioprinter. However, the BioBot did feature some advantages over the MakerBot bioprinter.

Table 1: Comparison of the MakerBot bioprinter and the BioBot printer platforms

	Makerbot bioprinter	**BioBot**
Extrusion mechanism	Pressure driven	Pressure driven
Pressure range	0-30 psi	0–120 psi
Number of extruders	1	2
Extrusion heating	--	RT–120˚C
Stage heating	RT–100˚C	--
Materials cross-linking capability	Blue light	Blue light
Designed for culture hood	--	☑
Culture plates compatibility	--	Petri dishes, 6/12/24/96-well plates

Critically, it had a larger extrusion pressure range, ability to heat and control the temperature of the extrusion mechanism and had programs specifically written for printing into culture plates, such as petri dishes and multi-well plates. Thus, due to the advantages and additions found in the BioBot system over the MakerBot bioprinter, we decided to employ the BioBot moving forward in the project.

In previously published studies, a variety of materials have been used as bioinks in bioprinting. Examples include synthetic and non-tissue specific materials such as alginate, gelatin, and collagen mixtures. However, these materials cannot represent the complexity of ECM and thus are inadequate to recreate a microenvironment with cell–cell connections and (3D) cellular organization that are typical of living skeletal muscle tissues [31]. Consequently, the cells in those hydrogels cannot exhibit intrinsic morphologies and functions of *in-vivo* living tissues.

It is thus ideal if cells are provided with a natural microenvironment similar to their parent tissue. We can reproduce that by using decellularized extracellular matrix (dECM). Recent studies actually showed the ability to isolate ECM from tissues, where by using chemicals and enzymes

specific to cellular components, we are able to strip away the cells from the tissue while maintaining the structural components of the tissue, which is ECM [13], [17].

Thus, for generating highly biomimetic skeletal muscle tissues, we selected skeletal muscle-dECM (sm-dECM) as our biomaterial. Previous studies were able to show that the use of dECM as the biomaterial actually improved maturation, survival and long-term function of engineered tissues [32], [33]. What makes dECM perfect for bioprinting is the fact that it can be initially extruded in liquid form under pressure but when incubated at 37˚C, it undergoes gelation which facilitates the retention of the printed 3D structure.

In order to recapitulate the structural organization of the 3D bioprinted tissues, uniaxial anchor point systems will be utilized. Such systems, where the engineered skeletal muscle tissues are suspended on both ends using rigid anchor structure. Several groups have shown that such systems induce passive tension on the suspended tissues, which influence the cellular structure to orient and align along the anchors' axis of tension [27], [34], [35].

2.2 METHODS AND MATERIALS

Decellularization of Skeletal Muscle

Freshly harvested porcine quadriceps and tibialis anterior muscles were sliced into approximately 25 mm^2 x 1 mm thick sections. Tissue sections were first washed in dI-H_2O for 1 hour before being placed in a solution of 1% SDS in PBS for 5 days. Tissues were then transferred to a solution of 0.1% Triton-X in PBS for 1 hour, followed by washes in PBS for 3 days. The decellularized skeletal muscle ECM (sm-dECM) were then lyophilized and stored for further use. To synthesize pre-gel solution, lyophilized sm-dECM is mixed with pepsin at a 10:1 mass ratio in a 0.1M HCl solution. This mixture was stirred until it became homogenous before it was brought to pH 7.4 with 10M NaOH and stored at 4°C in preparation for bioprinting.

Characterization of Mechanical Stiffness of the sm-dECM

Modulus measurements were obtained by compressing 5 mm-high cylinders of the 2% sm-dECM hydrogel in an Instron testing machine at a rate of 10 mm/min until failure.

Fabrication of PCL Structures

PCL beads (BioBot, USA) are first added to a 10mL stainless steel metal syringe fitted with a 30-gauge metal tip and loaded into the BioBot 1 printer's syringe holder. The syringe is then heated to a set temperature where the PCL is melted and the pressure is set to an appropriate level. The metal syringe is then allowed to equilibrate at the set temperature and all the PCL to melt. Using the BioBot software, the syringe tip is calibrated according to the manufacturer's protocol, where the tip is adjusted so that it sits just above the surface of the well bottom. The calibration and extrusion parameters are then verified to ensure proper dispensing of the PCL by depositing a drop on the surface. Subsequently, the PCL structures are printed according to the developed CAD. After all the PCL structures have been printed, they are inspected for any structural flaws or printing errors.

3D Bioprinting dECM Constructs

Solubilized dECM is loaded in a 10mL plastic syringe (BD, USA) fitted with a needle tip and loaded into the BioBot's syringe holder. Appropriate pressure is set using the BioBot software, where the deposition rate is optimal. Using the BioBot software, the extruder is centered and calibrated, where the needle is positioned just above the surface it is to be printed on. The dECM structures are subsequently printed at room temperature according to the appropriate CAD. The

printed dECM is assessed for structural integrity and print fidelity. Finally, the bioprinted dECM structures are incubated at 37˚C for 1 hour until gelled, at which point appropriate medium is supplied.

Developing of Computer Aided Design (CAD)

The designs for the 3D bioprinted structures will be developed using a 3D modeling software, Solidworks. The 3D models are then converted to a STereoLithography (STL) file format. Analogous to histologic sectioning, printing paths are created by "slicing" the STL models into individual 2D layers and creating tool paths that trace out the perimeter and interior features of each slice. The thickness of these layers is set to 0.2mm. These tool paths are the instructions read and executed by the bioprinting system for each layer. Layers are printed sequentially and stacked as the model is built up in an additive process forming a 3D object from the accumulation of 2D layers.

2.3 RESULTS AND DISCUSSION

2.3.1 *Design Iteration 1*

This design featured a simple 3D bioprinted band-like skeletal muscle tissue that is held on both ends by 2 circular PCL posts. Such anchor pair systems have been investigated by many previously published works and it has been shown that the anchor pair system is able to induce passive tension on the tissue, which influences the cellular orientation and alignment of the tissues [27], [36], [34]. The CAD for this design is shown below (**Figure 4A**).

First, the PCL post pairs were printed in a layer-by-layer process using the BioBot, where it was heated to 100˚C, extruded under 100 psi of pressure, and printed at 10 mm/s extruder speed. Once printed, the resultant PCL post pair structures showed a low degree of print fidelity (**Figure**

4B). The PCL posts specifically featured bending within the posts and string formation between them. More detailed inspection of the stacked layers showed inconsistent printing and shifted layer, which resulted in relatively unstable and unrepresentative structures of the designed models.

This inconsistent printing and structural artifacts that were observed within the printed structures were believed to be due to the extruder temperature at which the PCL was kept (100˚C). It was hypothesized that the PCL was indeed kept at a temperature at which it is melted, however, the temperature was low enough that as soon as it is extruded out of the nozzle, the PCL almost instantly solidified. Thus, after depositing a layer of one post, the extruder travels to the location to do the same, which results in pulling the just printed PCL along in the direction of travel, which results in the bending and string formation that was observed.

In response to this, the temperature at which the PCL extruder is kept should be increased by 10˚C to eliminate the structural variations and artifacts observed.

2.3.2 *Design Iteration 2*

This design featured 7 post-pairs with skeletal muscle tissue bands held between them (**Figure 5A**). This is essentially a multiple version of design 1, where the throughput of the system is increased. Similar to design one, the post pairs would induce passive tension on the muscle tissue bands, which would influence alignment and orientation of the cellular structures embedded in the printed bioink.

First, the PCL post pairs were printed in a layer-by-layer process using the BioBot 1, where it was heated to 110˚C, extruded under 100 psi of pressure, and printed at 10 mm/s extruder speed. However, regardless of the temperature change, the resultant PCL structure featured inconsistent and low fidelity printing. Structural bending and string formation were observed within the PCL

posts as can be seen in (**Figure 5B**). It was hypothesized at this time that these structural artifacts were due to two main factors: the extruder travel speed and the layer-by-layer printed process employed. Using a layer-by-layer process, the extruder prints the first layer of one post, travels to the location of the next and does the same, then travels to the next post and so on, until it returns to the first post and prints the second layer and repeats the process until all the objects are complete.

With this printing methodology, we observed that when extruding melted PCL and creating a layer of one post and travelling at a high speed to the next, the still melted PCL that had just been printed is pulled along with the extruder in the direction of travel, which would result in both bending and the formation of strings. In addition to the PCL print issues, it was observed that the bioink material did not adhere well to the circular posts but instead adhere to the surface of the plate instead. This results in tissue that is cultured on a stiff plastic surface and the intended passive tension induced by the posts would be absent.

In order to reduce and prevent the printed PCL structural issues, the extruder travel speed will be reduced from 10mm/s to 1mm/s, which would help limit the bending of the PCL posts. Additionally, the object will be printed in an object-by-object format instead of a layer-by-layer one, which means that each post is printed fully before printing the next one. This would reduce PCL formation of strings. Additionally, to ensure that the passive tension induced by the post pairs would influence cellular alignment and orientation, the tissues will have to be suspending above the culture plate.

To enable the fabrication of suspended tissue, the introduction of a sacrificial layer was required which would temporarily support the bioink until gelled then can be removed. Pluronic F127 was chosen for this purpose. Pluronic is a sacrificial material which can be extruded under

pressure but also retain its shape post printing at room temperature. The Pluronic can be utilized as a temporary sacrificial material because of the fact that when eluted by an aqueous solution, it is completely removed. These properties make it optimal for our bioprinting design.

Additionally, another factor of the printed skeletal muscle tissues that needed to be considered is the specific dimensions of the resultant constructs. A previous study which explored various post pair anchor systems with varying 3D muscle tissue dimensions found that constructs that feature a 3:1 aspect ratio of length: width of the tissue showed optimal influence on the cellular alignment and orientation of the resultant structures [37]. Thus, this aspect ratio will be incorporated into subsequent design models to optimize the influence of the passive tension on the cellular alignment of the skeletal muscle tissues.

2.3.3 *Design Iteration 3*

This design featured a cuff-like muscle tissue which features the 3:1 dimension aspect ratio that is printed on a Pluronic F127 sacrificial layer and suspended between 2 PCL walls. First, the PCL wall pairs were printed in an object-by-object process, where it was heated to 100˚C and extruded under 100 psi of pressure. Pluronic F127 was extruded as shown in (**Figure 6A**) at room temperature under 80 psi. Finally, the dECM bioink is deposited onto the Pluronic surface at room temperature using about 3 psi of pressure. All components of this design were printed with an extruder speed of 1 mm/s. The printed PCL wall structures were introduced in this model in order to increase the surface area of the PCL structures, which would facilitate better tissue-PCL adherence.

The PCL wall showed consistent layer stacking and no string formation or bending. In addition, the printed Pluronic and the dECM showed high fidelity contained constructs as can be

seen in (**Figure 6B**). Since a robust protocol of generating single muscle tissue models in a consistent and reproducible manner has been established and optimized, the CAD design can be expanded to bioprint multiple tissues in a multi-well culture plate to improve the throughput of the drug-screening system.

2.3.4 *Design Iteration 4*

In order to generate multiple tissues in a multi-well format, several factors need to be considered. Firstly, the extruder tip size must be accounted for so that when printing in a well, it does not intersect with the well walls or any of the previously printed structures. Additionally, future testing requirements need to be considered. In order to quantify functionality of the skeletal muscle tissues, they need to be electrically stimulated using a culture pacer apparatus, which is specifically designed for a 6-well culture plate. Due to these constraints, a design that is adapted for a 6-well culture plate is developed.

The design features 5 skeletal muscle tissues deposited on a Pluronic layer and held on both ends by 2 circular posts (**Figure 7A**). The components were printed with the same established printing parameters utilized in design 3.

The resultant printed components showed high fidelity and structural integrity as can be seen in (**Figure 7B**). However, one issue that did arise was bleeding between adjacent pre-gelled bioink structures. Moving forward, the bioprinted pre-gelled bioink structures must be better separated and contained to ensure optimal tissue formation and reduce secondary mechanical cues generated between adjacent post structures.

2.3.5 *Final Design*

This design featured improvements on the previously described model (design 4). The process of generating the skeletal muscle tissues is as follows. Firstly, PCL is melted to 100˚C and extruded under 100 psi pressure to generate 5 circular posts in an object-by-object process. It was observed the printed PCL posts are not very stably adhered to the culture plate surface. Consequently, any object that comes in contact with the post structures in subsequent printing actually broke-off and dislodged the PCL posts. In response, an ultra-violet (UV) curable resin, Norland Optical Adhesive 83H (NOA 83H) is subsequently bioprinted at room temperature under 3 psi of pressure using a 25-gauge needle to create a thin anchoring layer for the PCL posts. After UV curing for 4 hours, the NOA 83H layer facilitates the stabilization of the PCL post structures. Next, the Pluronic F127 sacrificial structure is bioprinted at room temperature under 80 psi of pressure using a 30-gauge needle. The Pluronic structure features a printed layer with 3 mm high walls on the NOA 83H layer, which would facilitate the separation of the pre-gelled bioink structures and the suspension of the printed muscle tissues. Lastly, the sm-dECM bioink is deposited within the Pluronic structures to generate skeletal muscle tissue constructs which feature a 3:1 (L: W) dimension aspect ratio and the resultant 3D bioprinted tissue is then incubated for 1 hour at 37˚C and allowed to crosslink. This procedure is repeated for each well within the 6-well culture plate as shown in (**Figure 8A**).

The resultant bioprinted PCL post pairs featured very consistent stacking of the individual layer with no structural variabilities or artifacts. The addition of the NOA 83H resin substantially improved the stability of the PCL structures, which ultimately facilitated in reproducibly generating this bioprinted system. The Pluronic printed structures were printed with very high precision exactly around the PCL posts, which created a contained space which the cell-laden sm-

dECM bioink can be deposited in. The gelled sm-dECM bioink was completely suspended in between the PCL posts, which would be influenced by the passive tension that is generated, resulting in aligned and highly oriented cellular structures which mimic the *in-vivo* structural characteristics of the native skeletal muscle tissues. Representative images of the printed system are shown below (**Figure 9**)

Ultimately, using a 3D bioprinting methodology as described above, we were able to show the development of a system which can be used to reproducibly and consistently generate 3-dimensional skeletal muscle tissues for their use in the drug discovery process as drug-screening assays. The fabrication process of these tissues is automated, which improves the accuracy, consistency, and reproducibility of generating these skeletal muscle tissues. In addition, we were able to demonstrate that with this technique, we are able to generate 5 tissues in every well of a 6-well culture plate (30 total tissue) in approximately 10 hours from start to finish. This is much faster than other techniques that our lab has utilized to produce such 3D tissues.

The following are the printing parameters and materials that were optimized and established.

Table 2: Established printing parameters of the various materials utilized

Material	Pressure	Extruder Temperature	Needle Size
Polycaprolactone (PCL)	100 psi	100 °C	30 gauge tip
Pluronic F-127	75-85 psi	25 °C	30 gauge needle
2% porcine sm-dECM	3-5 psi	25 °C	25 gauge needle
NOA 83H	< 3 psi	25 °C	20-25 gauge needle

2.4 SUMMARY

In summary, we demonstrated the development and optimization of a 3D bioprinting methodology for generating 3-dimensional skeletal muscle tissues. This approach utilized a uniaxial PCL post pair anchor system that induces passive tension along its axis, which consequently influences cellular alignment by orienting them along the axis of tension. Additionally, Pluronic F127 sacrificial layer was introduced in the design, which supports the suspension of the 3D bioprinted tissues above the culture plate surface to ensure the induction of the passive tension provided by the post anchors and eliminating the culture of the tissue on a stiff plastic environment. We also demonstrated the ability to extrude tissue specific dECM (sm-dECM) bioinks in a reproducible and consistent manner. In addition, in order to validate the mechanical properties on the 2% sm-dECM selected, stiffness measurements of 1.821 ± 0.137 kPa revealed that it is indeed on the same order of magnitude at the native skeletal muscle tissues (5-12 kPa [23]). Ultimately, we present an approach of generating *in-vitro* human 3-dimensional physiologically-relevant models that recapitulate aspects of the native skeletal muscle cellular microenvironment for the development of a reproducible and high-throughput drug-screening model in a rapid manner.

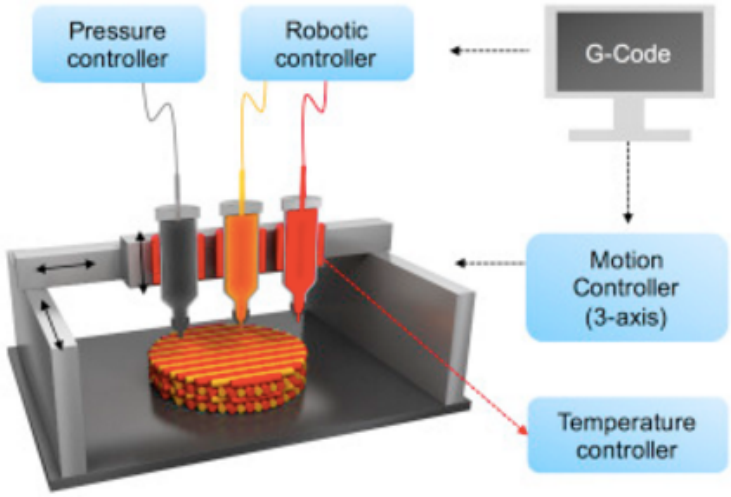

Figure 3: Illustration of a 3D bioprinting system, showing major components. Jang *et al.* Biomaterials 2017

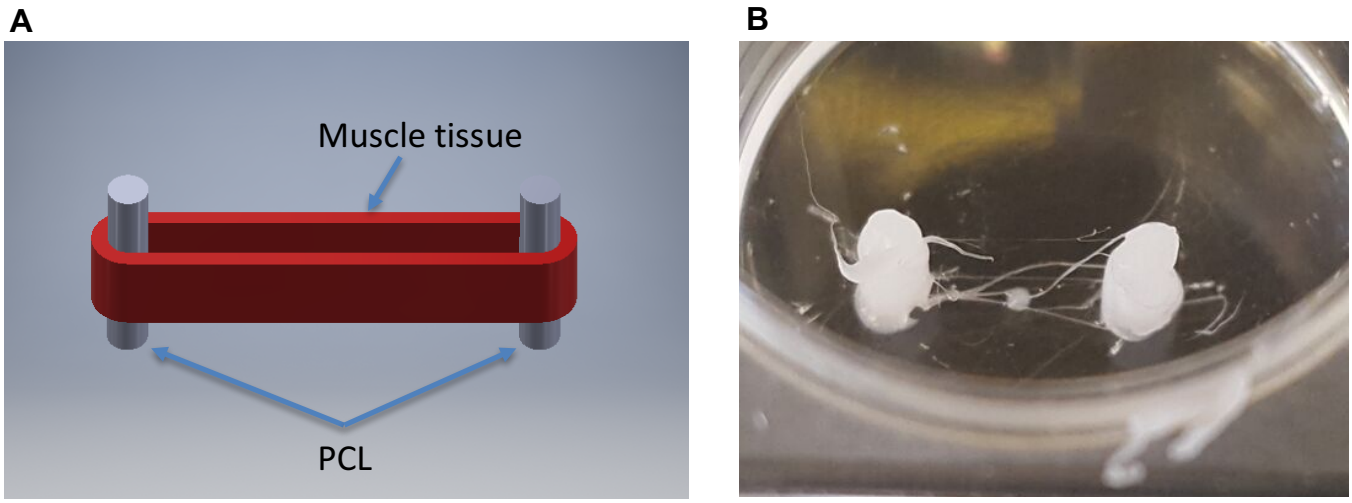

Figure 4: Prototype design iteration 1. (A) CAD model. (B) Representative image of resultant bioprinted structure

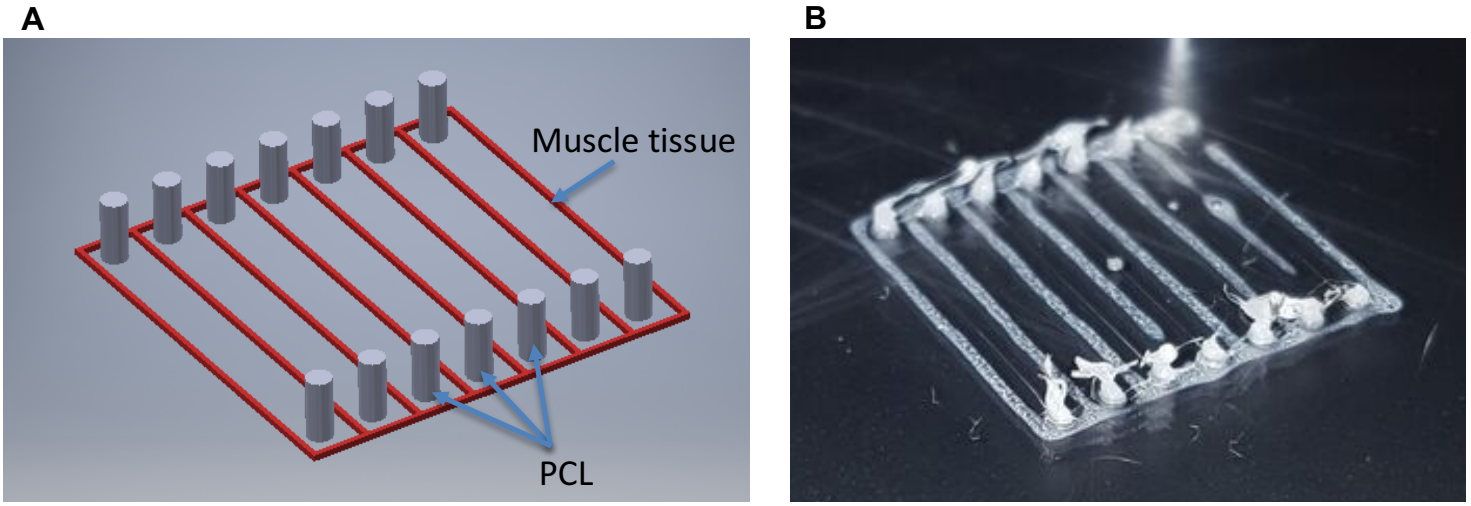

Figure 5: Prototype design iteration 2. (A) CAD model. (B) Representative image of resultant bioprinted structure

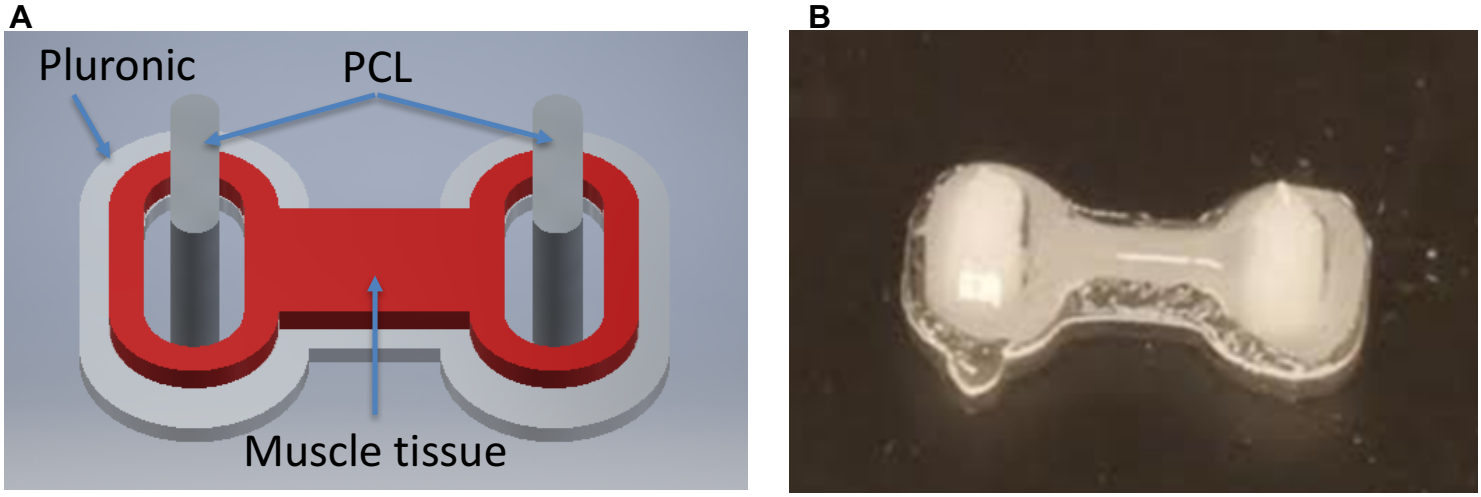

Figure 6: Prototype design iteration 3. (A) CAD model. (B) Representative image of resultant bioprinted structure

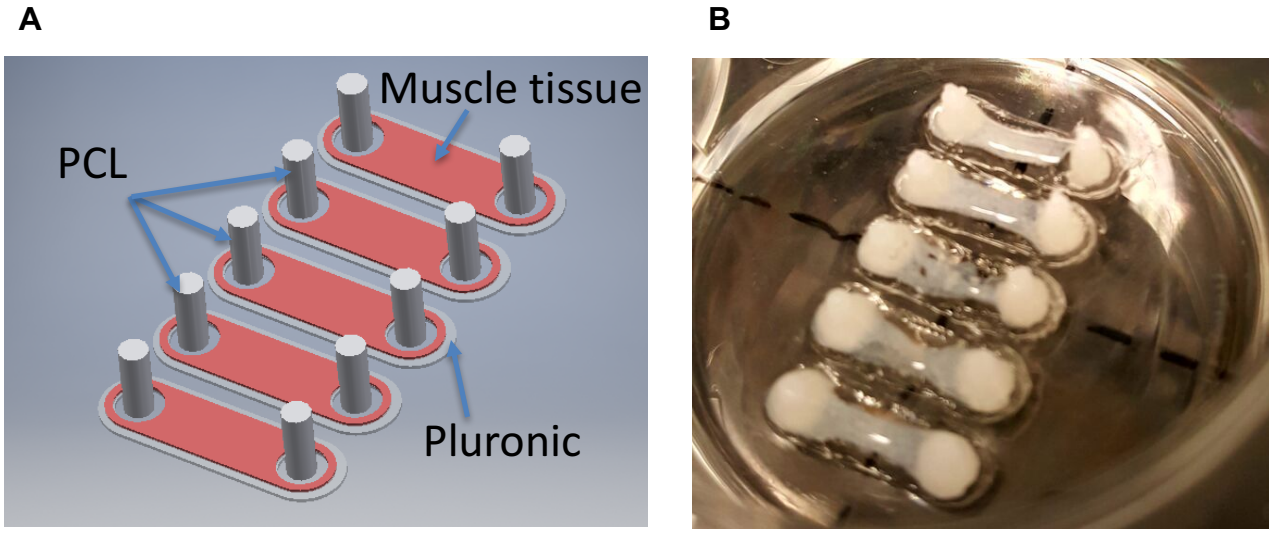

Figure 7: Prototype design iteration 4. (A) CAD model. (B) Representative image of resultant bioprinted structure

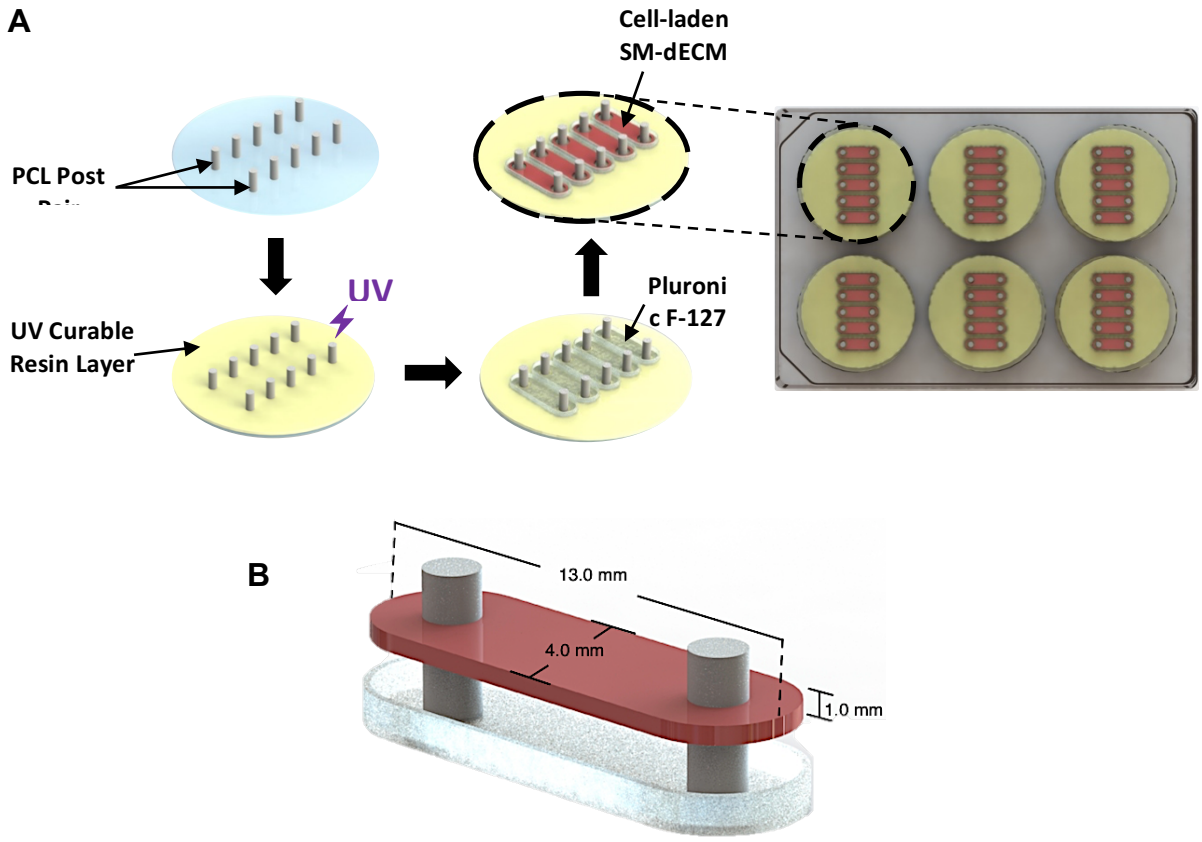

Figure 8: Printing process of skeletal muscle tissue constructs with dECM bioink. (A) First step involves printing a post structure using PCL. Next, a thin layer of NOA 83H is printed onto the dish surface and subsequently photo-crosslinked using UV light, which creates a stabilizing anchor for the PCL post structure. A sacrificial support structure is then printed using Pluronic F-127. Lastly, a cell-laden skeletal muscle derived dECM is printed onto the sacrificial support layer. The resultant 3D bioprinted tissue is then incubated and allowed to crosslink. This procedure is repeated for each well within a multi-well culture plate. (B) Exploded image of 3D bioprinted tissue showing dimensions of resultant structures.

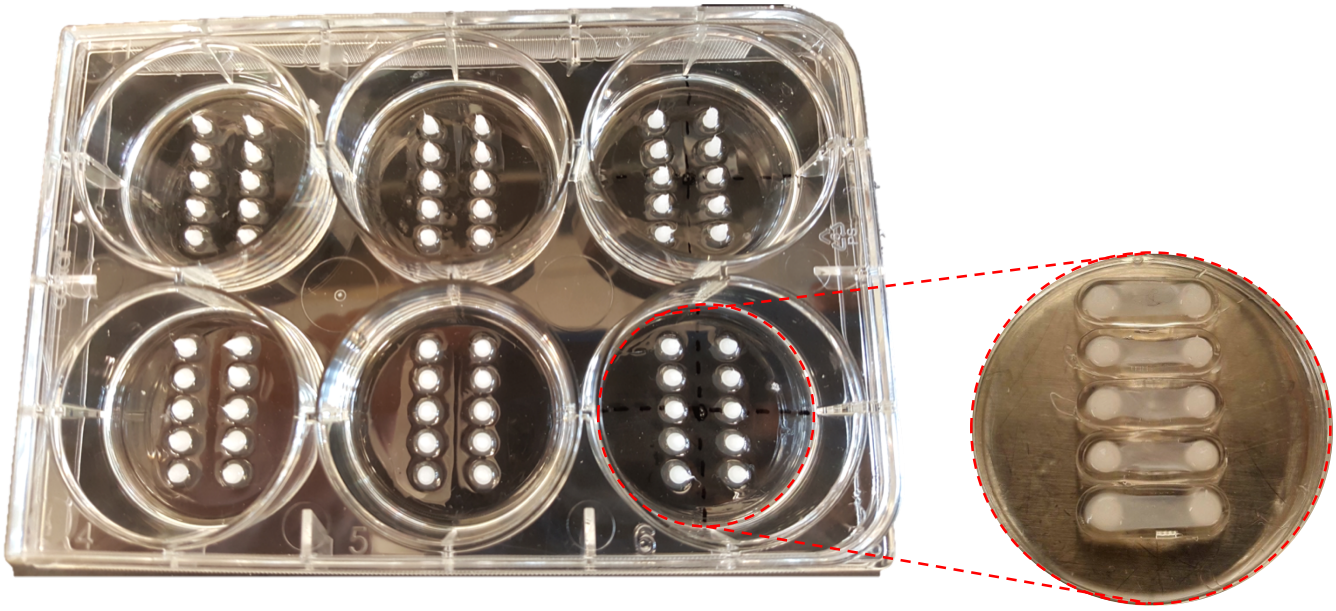

Figure 9: Representative images of the 3D bioprinted structures within a multi-well culture plate and of an individual 3D bioprinted tissue construct (inset)

Chapter 3. 3D Bioprint and Evaluate Structural and Functional Characteristics of Bioprinted Muscle Tissues

3.1 INTRODUCTION

During embryogenesis, the development of human skeletal muscle is coordinated with the development of many different organ systems, such as the skeletal system. It is widely believed that bone elongation directs the initial phases of muscle organogenesis [38]. Specifically, the continuous passive tension applied to skeletal muscle by bone influences muscle weight and length and myofilament organization [39]. In order to generate a physiologically relative biomimetic skeletal muscle tissue, it is imperative that this 3-dimensional organization is recapitulated in the engineered tissue. Many previously published studies have shown that this continuous passive tension can be reconstituted *in-vitro* by suspending the engineered muscle tissue between a uniaxial anchor system. The anchor points are then able to induce passive tension along the tissue, which influences the cellular structures to align and orient uniaxially parallel to the axis of tension. Thus, in this chapter, the effects of the post pair system proposed earlier on the alignment and orientation of the cellular structures of the 3D bioprinted tissues are assessed.

One concern of utilizing a 3D bioprinting approach for engineering tissues is the applied shear force exerted on the cells embedded in the bioinks due to the extrusion process [15], [17]. It is crucial that the bioinks should come out of the nozzle with minimum applied shear force; otherwise, the applied shear force may be substantial enough to cause damage to the cells and reduce the cell viability in the printed constructs. Thus, the viability of the cells within the 3D bioprinted constructs is measured.

Several previously published works that have generated skeletal muscle tissue using a 3D bioprinting technique have engineered the tissues utilizing non-human cell line and non-tissue

specific biomaterials. However, in order to generate an *in-vitro* tissue model that is physiologically relevant and highly biomimetic of that of the native skeletal muscle tissue, the various chemical, mechanical and physical cues found in the native tissue must be recapitulated. Here, we demonstrate the ability to 3D bioprint skeletal muscle tissues, using C2C12 or a human myoblast cell line and tissue specific dECM. Thus, in this chapter, the structural, maturity and functionality of the engineered skeletal muscle tissues will be investigated to assess the benefits of the proposed design and established protocol for 3D bioprinting these biomimetic humanized models.

3.2 Materials and Methods

Cell Culture Human Skeletal Muscle Myoblasts

HSMM were maintained in Skeletal Muscle Growth Media-2 (SkGM™-2 Medium), supplemented with human Epidermal Growth Factor [hEGF], Dexamethasone, L-glutamine, Fetal Bovine Serum [FBS], and Gentamicin/Amphotericin-B [GA]). Medium was replaced every 48 hours.

Printing and Culturing of HSMM-Laden Constructs

A BioBot 1 bioprinter is used for printing of cell-laden constructs. First, PCL is loaded in a metal syringe and heated to 100˚C to melt the polymer and subjected to 100 psi of pressure. The PCL post-pair structures are printed in an object-by-object process. Subsequently, a UV curable resin, NOA 83H is printed to stabilize and anchor the PCL posts to the plate's surface. The NOA 83H is then cross-linked under UV for 4 hours. The Pluronic F127 is printed according the established parameters discussed above in the format shown in the final design. Next, the HSMM-laden sm-dECM is bioprinted onto the Pluronic structure, which is then incubated at 37˚C for 1 hour then supplied with 3 mL of growth medium (Skeletal Muscle Growth Media-2 (SkGM™-2 Medium),

supplemented with human Epidermal Growth Factor [hEGF], Dexamethasone, L-glutamine, Fetal Bovine Serum [FBS], and Gentamicin/Amphotericin-B [GA]). Growth medium is replaced every other day for 5 days. On day 5 in culture, the growth medium is changed out to differentiation medium (high-glucose DMEM supplemented with 2% horse-serum and 1% Penicillin Streptomycin), which is replaced every other day for 10 days, at which point is changed and maintained in growth medium for 6 days.

Quantifying Cell Viability

In order to verify that the shear-stress that arises from the mechanical perturbations present due to the dispensing process, a live/dead assay was performed after the printing. The HSMM cells were encapsulated at a density of 10×10^6 cells/ml into 2% sm-dECM bioink and the prepared bioink was loaded into the syringe and placed within the BioBot printer. The previously described structure of the final design was printed at a pressure of ~ 3.0 psi at room temperature. Finally, the fabricated structure was allowed to crosslink by incubating at 37 °C temperature for 45 min and subsequently, 3mL of growth medium was added. After 48 h of incubation a Live/Dead staining was performed using the Live/Dead viability/cytotoxicity Kit (Molecular Probes, Inc., Eugene, OR) according to the manufacturer's instructions. In brief, calcein-AM and ethidium homodimer-1, were both added to 10 mL DPBS to create staining solution. The culturing media was aspirated from tissues and 1mL of the staining solution was added. Being an indicator of cell viability the calcein-AM is metabolically converted by intracellular esterase activity resulting in green fluorescent, calcein. However, ethidium homodimer-1 is excluded from live cells but is readily taken up by dead cells and stains the DNA. Tissues are then incubated in the staining solution for 45 min at 37°C after which time are immediately imaged.

Quantitative Analysis of Cell Alignment

To assess alignment, immunofluorescent images of phalloidin-stained cells were taken at 20x and 40x magnification and analyzed using a modified, previously published MATLAB script utilizing pixel gradient analysis [40]. In brief, the images were passed through a Gaussian low-pass filter and Sobel horizontal edge-emphasized filter (predefined MATLAB Image Analysis toolbox functions) to generate a 2D convolution. The Sobel filter was then transposed to extract the vertical edge, and the horizontal and vertical edges were combined to calculate the gradient magnitude of each pixel in the image. The image was then thresholded to determine the borders of the areas of interest, and the orientation of the gradient was calculated via respect to the x-axis (0˚). The orientation gradient data obtained from the pixel gradient analysis MATLAB script was then used to generate representative plots of overall cell alignment using a second custom MATLAB script. Each image was segmented into a grid of user-designated size. The gradient orientation angle for each pixel in a given grid square was then shifted in order to take a circular average with respect to the angle present with the highest incidence within that grid square's orientation angle data. This circular average is representative of the mean orientation of each pixel gradient within a given grid square.

Imaging Calcium Sparks in Human Skeletal Muscle Myoblasts

4.5 uM fluo-4 AM was prepared in growth medium and added to the skeletal muscle tissues, which were subsequently incubated at 37˚C. After, a 5-minute wash with Tyrode’s solution was repeated 3 times, while kept in the dark at room temperature. Fluo-4 AM-loaded tissues are then kept in Tyrode’s solution and Ca2+ transients will be elicited by field stimulation using 2 parallel electrodes (6-well C-dish, IonOptix Inc.) with voltage pulses delivered by an electrical stimulator

(C-Pace EP, IonOptix Inc.). Tissues were stimulated with 10.0V at 1.0Hz and duration of 20.0ms. During which, confocal images of the calcium fluorescence were taken at 40x magnification and the calcium transients regions were identified and designated as the regions of interest. Subsequently, fluorescence intensities were plotted and several measurements were taken from regions were the calcium sparks were observed and compared to the background fluorescence.

Immunohistological Study

The 3D bioprinted structures were embedded in OCT compound on day 21 of culture and sectioned using Cryotome in 10-µm thickness. The samples were fixed with a solution of 4% paraformaldehyde for 10 minutes and washed 3 times in PBS and then permeabilized with a solution of 0.2% Triton X-100 and 5% normal goat serum (NGS) in PBS for 1 hour at room temperature. They were then incubated overnight at room temperature with a mouse anti-human all isoforms myosin heavy chain primary antibody diluted 1 in 10 in PBS (+2% NGS and 0.2% Triton X-100). After overnight incubation, the samples were washed thoroughly in PBS before being treated with a goat anti-mouse Alexa Fluor 594 secondary antibody (Invitrogen) diluted 1 in 300 in PBS (+2% NGS and 0.2% Triton X-100), as well as phalloidin-FITC diluted 1 in 300 in PBS (+2% NGS and 0.2% Triton X-100) for 3 hours at room temperature in a darkened chamber. Subsequently, the samples were washed thoroughly in PBS. The nuclei were stained using DAPI-containing MOWIOL mounting medium, which was applied to the samples before mounting with a cover slip. Any excess solutions are wiped away and a thin layer of clear nail polish is applied to the sides of the cover slip to seal the samples. Cells were visualized a confocal microscope and accompanying software.

Gene Expression Analysis

The 3D bioprinted tissues and 2D controls were harvested at day 21, and the total RNA of cells was isolated using E.Z.N.A Total RNA Kit following the manufacturer's instructions. After the extraction of the RNA, cDNA was prepared using a iScript Reverse Transcription Supermix (Bio-Rad, USA) following the manufacturer's protocol. The expression levels of relative myogenic differentiation genes (*MYH2, MYH3, MYH8, TNNI1, PAX7, MYF5*, and *MYOD1*) were analyzed with SYBR-green using a CFX96 Real-Time PCR system (Bio-Rad, USA). The expression levels for the target gene were normalized with an endogenous glyceraldehyde 3-phosphate dehydrogenase control using the $2^{(-\Delta\Delta CT)}$ method.

3.3 Results and Discussion

Quantitative Analysis of Cell Alignment within C2C12-Laden Skeletal Muscle Tissues

In order to validate the design of the proposed methodology of generating 3D skeletal muscle tissues, 3D bioprinting of 2% (w/v) sm-dECM embedded with C2C12–an immortalized mouse myoblast cell line–was performed. The tissues were generated by using a cell density of $20x10^6$ cell/mL of 2% sm-dECM, which were cultured for 21 days and analyzed for cellular alignment and orientation within the tissue.

Immunofluorescent staining of cellular cytoskeletal proteins (F-actin) indicated that cells within the 3D bioprinted skeletal muscle tissues demonstrated a well-aligned cellular cytoskeleton (**Figure 10A**). Automated image analysis was used to quantify alignment of the cells embedded within the sm-dECM hydrogels on day 21 of culture. The tissues demonstrated significant structural alignment along the tension axis (0˚) generated by the post pair structures, represented by the yellow arrow (**Figure 10B**). This highly aligned cellular structure is biomimetic of the cellular structure that is observed in the native skeletal muscle tissues in the human body. These

results indeed validated the proposed system and design for the generation of 3-dimensional skeletal muscle tissues, which feature highly aligned and organized cellular structures.

3D Bioprinting Human Skeletal Muscle Tissues

Since the proposed system and design of generating skeletal muscle tissues was validated with the C2C12 mouse cell line, 3D bioprinting of human skeletal muscle tissues was subsequently attempted. Human skeletal muscle myoblasts (HSMM)–isolated from the upper arm or leg muscle tissue of normal human donors–were embedded in 2% sm-dECM at a density of $10x10^6$ cells/mL. This specific cell encapsulation density was utilized instead of the $20x10^6$ cells/mL density utilized with the C2C12 is because it was observed that the tissues with the higher cellular density were prone to snapping in culture. It was hypothesized that at this density, enough force is generated by the cells to result in snapping of the tissue, thus utilizing a lower cell density would be optimal for generating and maintaining the skeletal muscle tissues.

The 3D bioprinted human skeletal muscle tissue structures are maintained in culture for 21 days, at which point the tissues are analyzed for several end points.

Quantification of Cellular Viability Within 3D Bioprinted Skeletal Muscle Tissues

For printing of cell-laden dECM, an important criterion is that the material should be extruded out of the nozzle with minimum applied shear force on the embedded cells. Otherwise, the applied shear force may cause damage to the cells and reduce the cell viability in the printed tissues. Thus, the viability of the cells within the printed tissues was assessed using a live/dead stain 24 hours post-print (**Figure 11**). The results demonstrated that the tissues featured very high cell viability

of about 96%, which suggests that shear stress exerted on cell is not sufficient enough to induce cellular damage or death.

Quantitative Analysis of Cell Alignment Within HSMM-Laden Skeletal Muscle Tissues

It is expected that through the designed PCL post anchor system, passive tension would be induced along the 3D bioprinted tissues and the cellular alignment and orientation would be influenced. In order to assess the cellular structural organization of the 3D bioprinted human skeletal muscle tissues and compare it with the native *in-vivo* tissue, cellular alignment quantification was analyzed. Immunofluorescent staining of cellular cytoskeletal proteins (F-actin) indicated that cells within the 3D bioprinted skeletal muscle tissues demonstrated a well-aligned cellular cytoskeleton (**Figure 12A**). Similar to the protocol utilized in earlier C2C12 image analysis, automated image analysis was used to quantify alignment of the cells embedded within the sm-dECM hydrogels on day 21 of culture. The findings demonstrated that the tissue showed significant structural alignment along the tension axis (0˚) generated by the post pair structures, represented by the yellow arrow (**Figure 12B**). The highly aligned cellular structure found in the 3D bioprinted human skeletal muscle tissues is biomimetic of the cellular structure that is observed in the native skeletal muscle tissues in the human body.

It was observed from the F-actin stains of the 3D human bioprinted tissues is that the cell density seemed relatively low. When cellular density is sparse, the human myoblasts might not be close enough to where they are able to fuse and form myotubes. In order to assess myotube formation within the 3D human bioprinted skeletal muscle tissues, a myosin heavy chain stain was performed according to the method described previously. Analysis of the fluorescence images

revealed a negative MHC stain, which does indeed suggest that there was a lack of myotube formation (**Figure 13**).

Tissue-Specific Gene Expression

The beneficial effect of sm-dECM bioink and the 3D development of the tissues were investigated by assessing tissue-specific myogenic differentiation state. Gene expression was evaluated through a quantitative real-time polymerase chain reaction (qRT-PCR), which was run on 3 experimental groups on day 21 of culture: 1) 3D bioprinted human skeletal muscle tissues (HSMM embedded in 2% sm-dECM), 2) HSMM cultured on 2D plastic, 3) HSMM cultured on 2D 2% sm-dECM. For each group, the following gene expression levels were measured: *TNNI1, MYH2, MYH3, MYH8, PAX7, MYF5,* and *MYOD1*. *TNNI1* is the gene that codes for the protein troponin I that is found slow skeletal muscle. *MYH2,3,8* are genes that specifically code for multiple isoforms of the protein myosin heavy chain (MHC), which are ATP-dependent motor proteins that are involved in muscle contraction. *PAX7* is a gene that codes for paired box protein (Pax-7), which is involved in in neural crest development and gastrulation. *MYF5* and *MYOD1* expression activates MyoD expression, which is retained in the proliferation and differentiation of progeny in the myogenic differentiation process. The expression of the contractile markers (*TNNI1, MYH2, MYH3,* and *MYH8*) is an indication of more advanced myogenic differentiation and maturation, while expression of the early myogenic developmental markers (*PAX7, MYF5,* and *MYOD1*) is indicative of a relatively immature myogenic state [41].

Figure 14 shows the relative gene expression levels of the 2D culture of HSMM on dECM in comparison to 2D culture of HSMM on plastic (represented by the red line). The results showed that there was an up-regulation of the contractile protein markers (*TNNI1, MYH2, MYH3,* and

MYH8) and down-regulation of the early myogenic markers (*PAX7, MYF5, MYOD1*). These finding suggest that the presence of the tissue-specific sm-dECM enhanced maturation of the human myoblasts.

This test was also run on the human 3D bioprinted tissues; however, there was difficulty in extracting high quality RNA from the dECM hydrogel and had high levels of protein contamination. Thus, the resultant data was inconsistent from this group. However, current efforts are made for optimizing a protocol for effective extraction of RNA to analyze for myogenic-specific maturation state.

Calcium Imaging Of 3D Bioprinted Human Skeletal Muscle Tissues

In order to investigate the functionality of the 3D bioprinted skeletal muscle tissue, calcium sparks were investigated. The 3D tissues were loaded using a Fluo-4 AM dye, which exhibits increased florescence upon binding to calcium. Thus, it is expected when the dye-loaded skeletal muscle tissues are electrically stimulated, calcium would be released from the sarcoplasmic reticulum, where it would bind to the Fluo-4 dye and fluoresce. However, when this test was run on the 3D bioprinted human tissues, no fluorescence signal was detected. This suggest that the tissues did not have any myotube formations. This further validates the hypothesis that the cellular density within the 3D human skeletal muscle tissues was low. However, we were interested in validating the calcium dye loading protocol for the HSMM, thus the same protocol and test was run on 2D cultured HSMM on nano-patterned topography, which influences cellular alignment. As can be seen from the plot (**Figure 15**), with the 2D group a fluorescence signal was detected in correspondence with the electrical stimulation, which validated the protocol utilized for loading the human myoblasts with the calcium dye.

3.4 SUMMARY

In summary, we were able to demonstrate the ability to 3D bioprint highly viable human skeletal muscle tissues, which feature highly aligned, oriented cellular structures, which is mimetic of what is observed in human native tissues. Additionally, by comparing myogenic marker expression levels between human myoblasts cultured on plastic and human myoblasts cultured on sm-dECM, we showed that the presence of tissue-specific biomaterial in culture enhances the maturation of muscle cells. As can be observed from the immunofluorescence stains of the 3D bioprinted skeletal muscle tissues, the cell encapsulation density is low, which limits the cells ability to fuse and form myotubes. Thus, for future experiments, it is recommended that the cell encapsulation density is increased to 15-20x10^6 cells/mL. Subsequent MHC stains should be performed to assess myotube formation, and calcium imaging should be performed on the 3D human bioprinted tissues to investigate functionality. Additionally, the time point at which the growth medium is replaced with a differentiation medium should be investigated more closely and optimized. This is a critical point in the culturing process. If the differentiation medium is introduced too early, the myoblasts might be close enough to each other, thus, are unable to fuse and form myotubes. On the other hand, it the differentiation medium is introduced later than optimal, the cells might have remodeled the sm-dECM significantly to a point that the cells' environment becomes too rigid for the myoblasts to fuse and form myotubes.

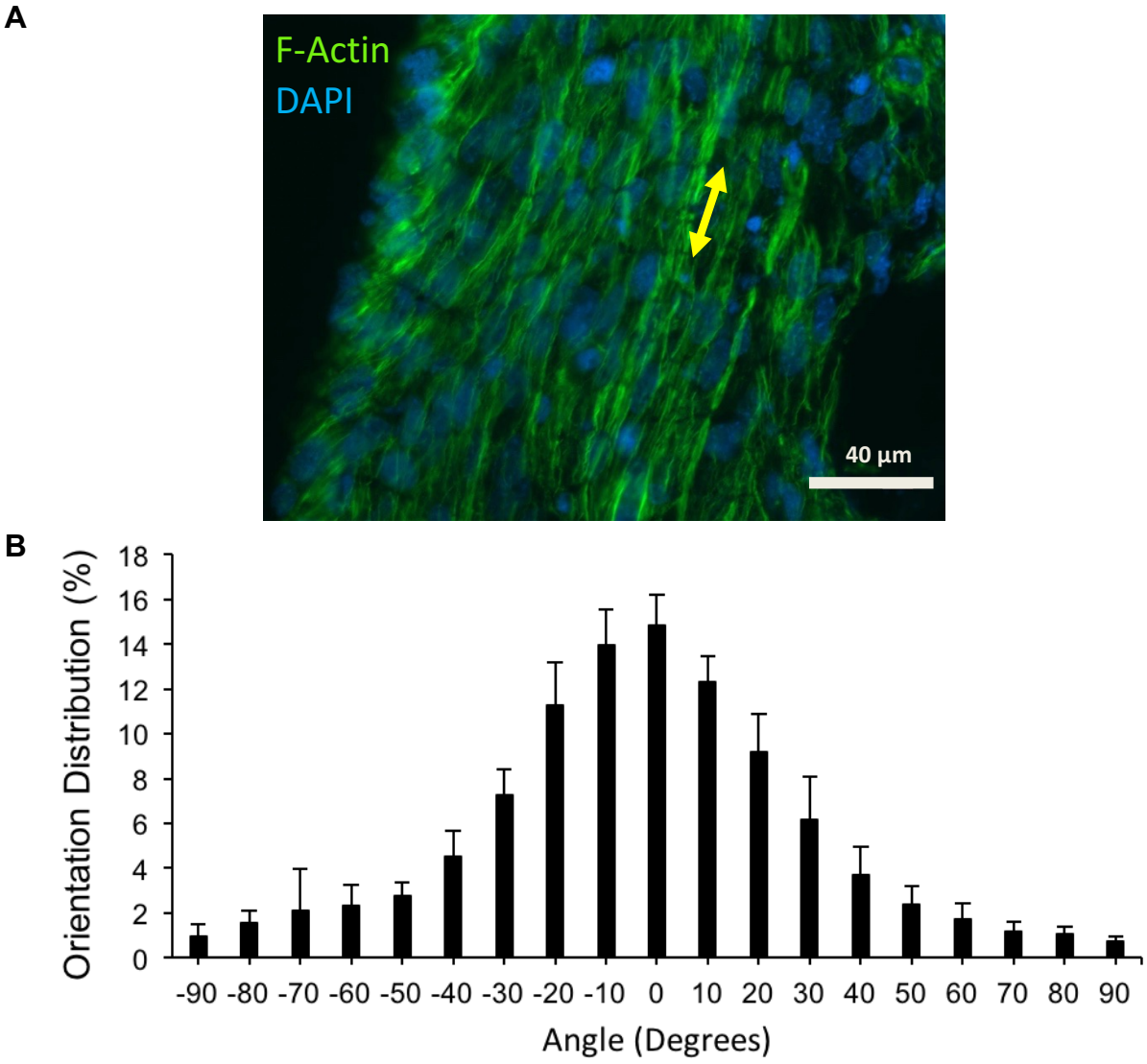

Figure 10: Immunofluorescent image of bioprinted C2C12 constructs and quantification of cellular alignment. (A) Representative fluorescent images of C2C12 cells cultured within 3D dECM construct seeded at 20 million cells/ml at 21 d. Cells were stained F-actin (green), and nuclei (blue). Yellow arrow indicates the axis of tension induced by the post pairs. (B) Quantitative analysis of overall orientation of cells cultured within the 3D bioprinted muscle tissues after 21d as performed by using a MATLAB script, where 0˚ corresponds to axis of post pairs

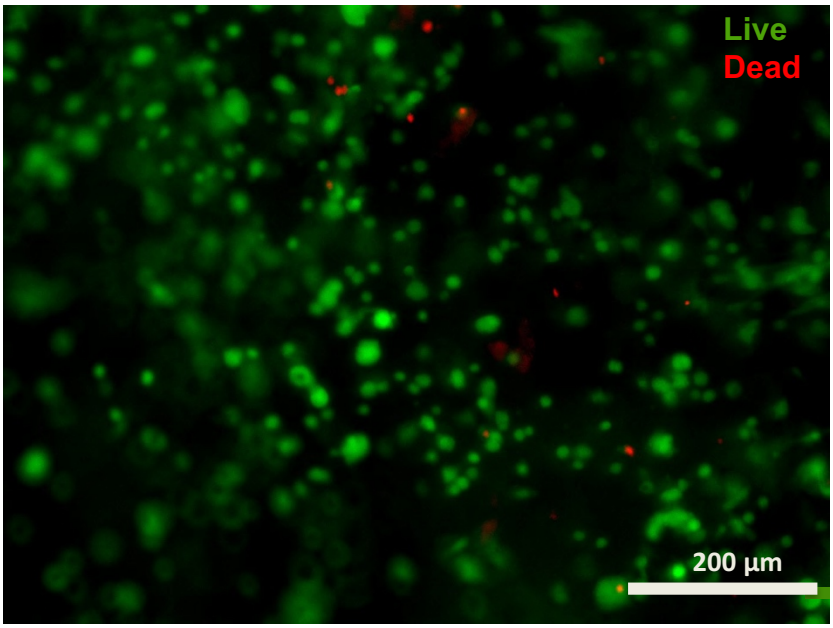

Figure 11: Results of Live/Dead cell assay. Cell viability of HSMM cells 48 h post printing was assessed using Live/ Dead staining. Live cells were measured by the enzymatic conversion of permeant calcein-AM to fluorescent calcein (green). Dead cells were detected by the uptake of ethidium bromide into cell DNA (red). Test indicated an average viability of 95.8% with a standard deviation of 1.51%.

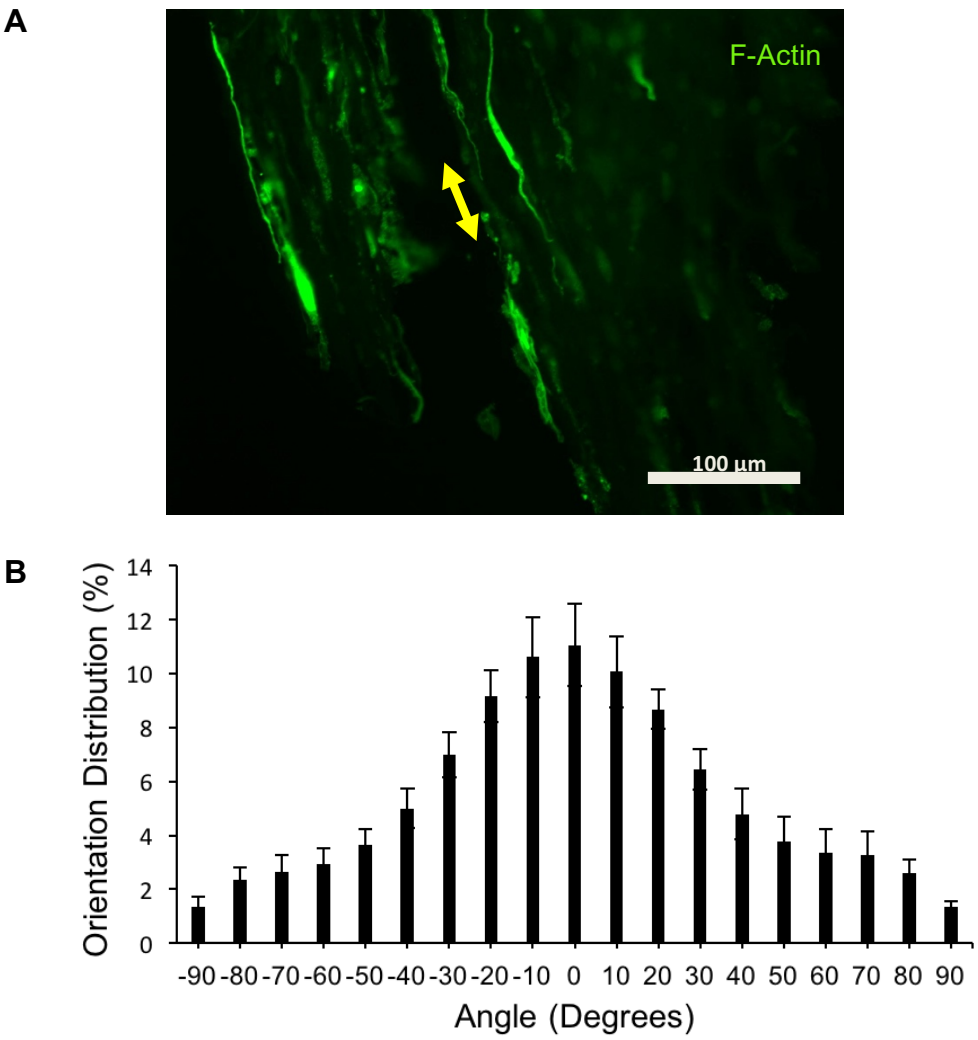

Figure 12: Immunofluorescent image of the bioprinted human skeletal muscle tissues and quantification of cellular alignment. (A) Representative fluorescent images of HSMM cells cultured within 3D dECM construct seeded at 10 million cells/ml. Cells were stained F-actin (green). (B) Quantitative analysis of overall orientation of cells cultured within the 3D bioprinted muscle tissues after 21d as performed by using a MATLAB script, where 0˚ corresponds to axis of post pairs

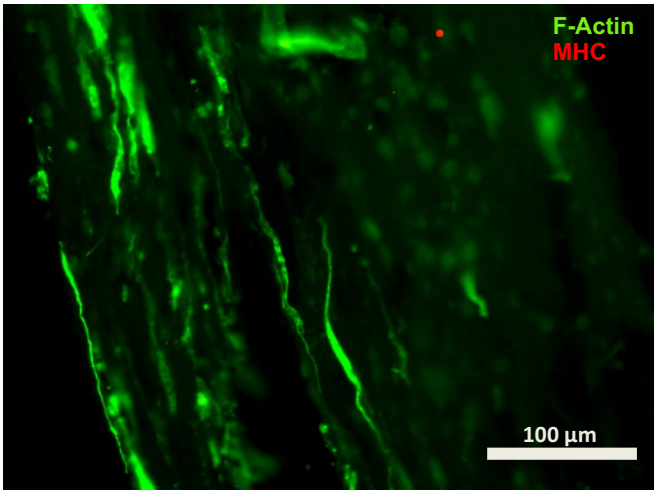

Figure 13: Immunofluorescent image of the bioprinted human skeletal muscle tissues. stained for both F-Actin and MHC. Cells were stained for F-Actin (green) and MHC (red).

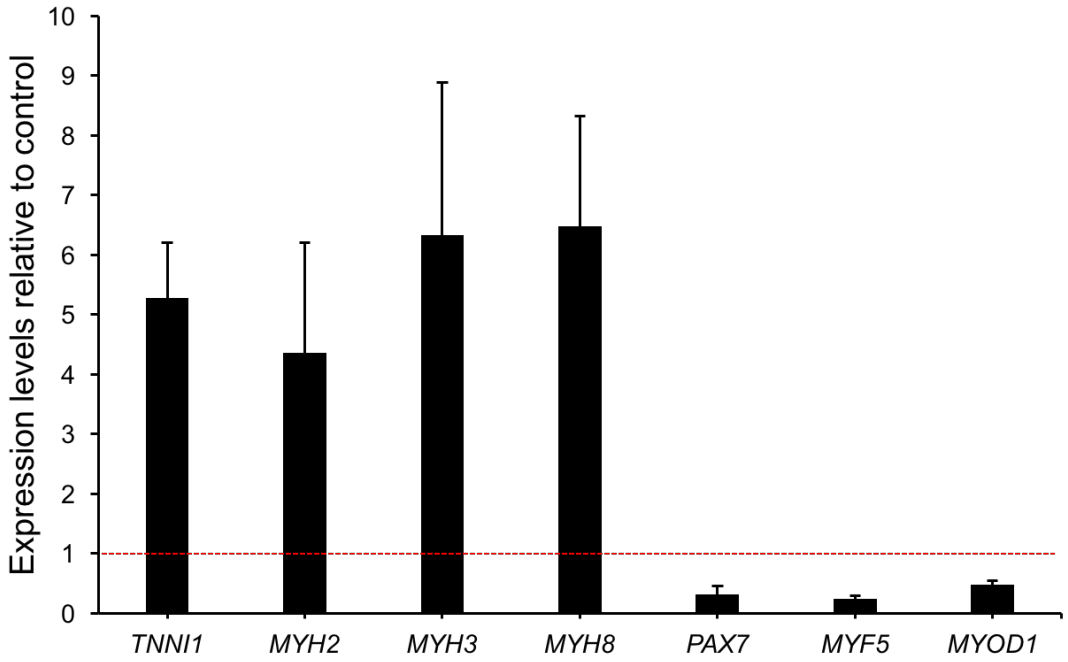

Figure 14: Skeletal muscle cell marker gene expression by qRT-PCR. Plots compare 2D HSMM culture on plastic, and 2D HSMM culture on sm dECM gene relative expression of early (*PAX7, MYF5, and MYOD1*) and late (*TNNI1, MYH2, MYH3, and MYH8*) muscle cell markers, normalized to *GAPDH*. Data is presented as means ± SEM, n = 3.

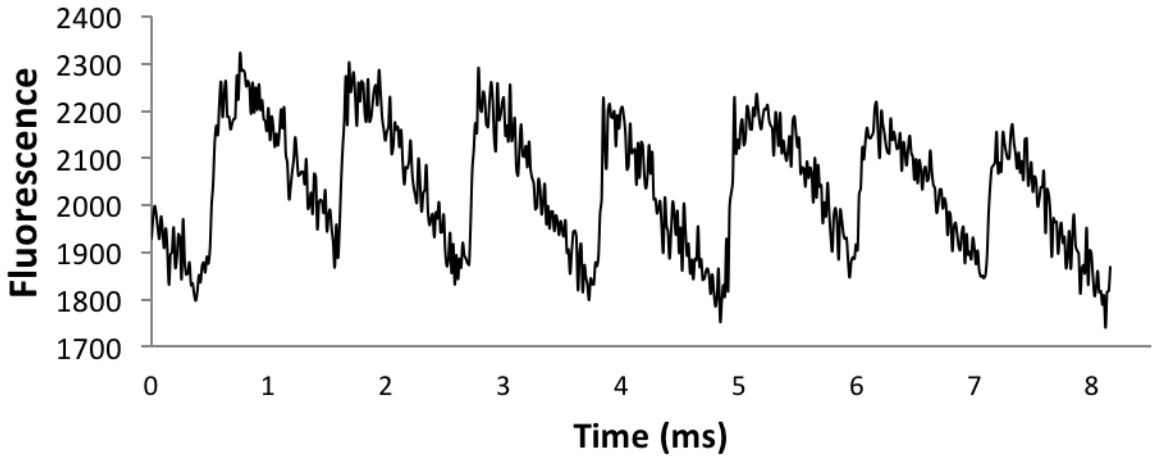

Figure 15: Calcium transience within HSMM cells. Representative intracellular calcium signals trace of a Fluo-4-loaded HSMM 2D monolayer cultured on nanopattern substrate at day 5 in differentiation media following repetitive electrical stimulation (10V, 1.0Hz, 20.0 ms).

Chapter 4. Conclusions

In this study, we demonstrate the development and optimization of a 3D bioprinting tissue engineering approach for generating *in-vitro* 3D humanized skeletal muscle tissues that recapitulate aspects of the native cellular microenvironment for the development of a reproducible and high-throughput drug-screening model. First, we selected optimal materials and bioinks that can be utilized in 3D bioprinting. In order to recapitulate the chemical and mechanical characteristics found in the native tissues, sm-dECM was utilized as the biomaterial due to containing a variety of the native ECM components. Also, PCL was selected to introduce rigid uniaxial anchor points, which the muscle tissue would be suspended between resulting in continuous passive tension induction along the tissue. This passive tension anchor systems have been shown to influence the alignment and orientation of the cellular structures embedded within the engineered tissues. PCL was specifically chosen due to having a relatively low melting point in comparison to other plastics, which is advantageous when using a bioprinting platform that is limited by extruder temperature control. Next, several parameters utilized in the bioprinting process were optimized. Specifically, the temperature that the extruder is kept at, the pressure utilized to extrude the various materials, extruder traveling speeds, and extruder needle sizes. In addition, several CAD designs were generated to 3D bioprint the skeletal muscle tissue structures. The final model featured a high throughput design, where multiple tissues are fabricated in a multi-well format. Each tissue is suspended in between two rigid anchors, which influence the cellular alignment and orientation along the axis of tension. Utilizing such a high throughput design for generating 3D skeletal muscle tissues is especially advantageous in an application such as drug-screening. The generation of the tissue constructs in a 6-well format allows investigators to test

several drugs or various doses of a drug concurrently to obtain data about the effects of the compounds in a relatively rapid manner.

The design of the system was initially validated by bioprinting C2C12-laden sm-dECM to generate rodent skeletal muscle tissue constructs. Quantification of the cellular alignment within the bioprinted tissue structures revealed that the tissue featured highly aligned tissue structures along the anchors' axis of tension. Subsequently, the tissue models were bioprinted using HSMM-laden sm-dECM to generate humanized 3-dimensional tissues. Firstly, the viability of the printed tissues was investigated. The results showed that the human skeletal muscle tissues featured high cellular viability of about 96%. This result suggests that the bioprinting extrusion process itself does not produce sufficient shear force to cause cellular damage our death. Next, cellular alignment was investigated within the human skeletal muscle tissues and the results indicated that high cellular alignment was achieved within the tissues, which are specifically oriented along the axis of tension generated by the rigid uniaxial anchor points. This structural organization is mimetic of that observed in the native human skeletal muscle tissues *in-vivo*. Next, the selection of the sm-dECM material as the bioink was validated by investigating its effects on enhancing the maturation of the human myoblasts. Relative myogenic expression markers were compared between HSMMs cultured on sm-dECM and HSMMs cultured on plastic. qRT-PCR data showed an up-regulation of contractile proteins markers and down-regulation of early myogenic markers. These findings suggest that the presence of the sm-dECM enhanced that maturation of the human myoblasts. However, future experiments that investigate the cellular maturation within the 3D bioprinted human skeletal muscle tissues must be performed.

Once the biological parameters have been optimized, this approach can be utilized to generate *in-vitro* humanized skeletal muscle tissue models that can be implemented as drug-

screening platforms. In order to validate the tissues and assess their efficacy and accuracy in predicting possible drug effects, validation tests must be performed. Initially, a compound that triggers a known specific response in the native skeletal muscle tissue *in-vivo* can be introduced to the 3D bioprinted models. Thus, for an example, if acetylcholine, a compound that increases contraction frequency of the *in-vivo* skeletal muscles, is introduced, we would expect a similar response in the 3D bioprinted tissues. After the validation steps have been complete, the 3D bioprinted skeletal muscle tissue platform can be used as a predictive tool for accurately determining the efficacies and possible toxicities a drug might have in the human body.

BIBLIOGRAPHY

[1] S. Morgan, P. Grootendorst, J. Lexchin, C. Cunningham, and D. Greyson, "The cost of drug development: A systematic review," *Health Policy*, vol. 100, no. 1. pp. 4–17, 2011.

[2] J. P. Hughes, S. Rees, S. B. Kalindjian, and K. L. Philpott, "Principles of early drug discovery.," *Br. J. Pharmacol.*, vol. 162, no. 6, pp. 1239–49, Mar. 2011.

[3] A. I. Baras, A. S. Baras, and K. a. Schulman, "Drug development risk and the cost of capital," *Nat. Rev. Drug Discov.*, vol. 11, no. April, pp. 347–348, 2012.

[4] J. W. McGreevy, C. H. Hakim, M. A. McIntosh, and D. Duan, "Animal models of Duchenne muscular dystrophy: from basic mechanisms to gene therapy," *Dis Model Mech*, vol. 8, no. 3, pp. 195–213, 2015.

[5] A. S. T. Smith, J. Davis, G. Lee, D. L. Mack, and D. H. Kim, "Muscular dystrophy in a dish: engineered human skeletal muscle mimetics for disease modeling and drug discovery," *Drug Discov. Today*, vol. 21, no. 9, pp. 1387–1398, 2016.

[6] H. Bart van der Worp, D. W. Howells, E. S. Sena, M. J. Porritt, S. Rewell, V. O'Collins, and M. R. Macleod, "Can animal models of disease reliably inform human studies?," *PLoS Med.*, vol. 7, no. 3, pp. 1–8, 2010.

[7] R. Greek and A. Menache, "Systematic reviews of animal models: Methodology versus epistemology," *International Journal of Medical Sciences*, vol. 10, no. 3. pp. 206–221, 2013.

[8] T. A. Partridge, "The mdx mouse model as a surrogate for Duchenne muscular dystrophy," *FEBS Journal*, vol. 280, no. 17. pp. 4177–4186, 2013.

[9] B. R. MacIntosh, P. F. Gardiner, and A. J. McComas, *Skeletal muscle : form and function*. Human Kinetics, 2006.

[10] A. R. Gillies and R. L. Lieber, "Structure and function of the skeletal muscle extracellular matrix," *Muscle Nerve*, vol. 44, no. 3, pp. 318–31, 2011.

[11] T. H. Petersen, E. A. Calle, L. Zhao, E. J. Lee, L. Gui, M. B. Raredon, K. Gavrilov, T. Yi, Z. W. Zhuang, C. Breuer, E. Herzog, L. E. Niklason, J. B. Orens, E. R. Garrity, H. C. Ott, T. W. Gilbert, T. L. Sellaro, S. F. Badylak, P. M. Baptista, M. R. Inanlou, M. Baguma-Nibasheka, B. Kablar, J. L. Sporty, L. HorÃ¡lkovÃ¡, C. Ehrhardt, D. Massaro, N. Teich, S. Maxwell, G. D. Massaro, P. Whitney, C. F. Andrade, A. P. Wong, T. K. Waddell, S.

Keshavjee, M. Liu, J. Cortiella, M. J. Mondrinos, H. Sugihara, S. Toda, S. Miyabara, C. Fujiyama, N. Yonemitsu, Y. M. Lin, A. R. Boccaccini, J. M. Polak, A. E. Bishop, V. Maquet, P. Macchiarini, D. O. DeFouw, T. E. Gray, K. Guzman, C. W. Davis, L. H. Abdullah, P. Nettesheim, D. Wang, J. E. Morales, D. G. Calame, J. L. Alcorn, R. A. Wetsel, J. Yu, C. F. Kim, H. J. Rippon, and B. Roszell, "Tissue-engineered lungs for in vivo implantation.," *Science*, vol. 329, no. 5991, pp. 538–41, 2010.

[12] B. E. Uygun, A. Soto-Gutierrez, H. Yagi, M.-L. Izamis, M. A. Guzzardi, C. Shulman, J. Milwid, N. Kobayashi, A. Tilles, F. Berthiaume, M. Hertl, Y. Nahmias, M. L. Yarmush, and K. Uygun, "Organ reengineering through development of a transplantable recellularized liver graft using decellularized liver matrix.," *Nat. Med.*, vol. 16, no. 7, pp. 814–20, Jul. 2010.

[13] H. C. Ott, T. S. Matthiesen, S. Goh, L. D. Black, S. M. Kren, T. I. Netoff, and D. A. Taylor, "Perfusion-decellularized matrix : using nature ' s platform to engineer a bioartificial heart," vol. 14, no. 2, pp. 213–221, 2008.

[14] L. E. Flynn, "The use of decellularized adipose tissue to provide an inductive microenvironment for the adipogenic differentiation of human adipose-derived stem cells," *Biomaterials*, vol. 31, no. 17, pp. 4715–4724, 2010.

[15] B. Derby, "Printing and prototyping of tissues and scaffolds.," *Science*, vol. 338, no. 6109, pp. 921–6, 2012.

[16] W. Yeong, C. Chua, K. Leong, and M. Chandrasekaran, "Rapid prototyping in tissue engineering : challenges and potential," vol. 22, no. 12, 2004.

[17] F. Pati, J. Jang, D.-H. Ha, S. Won Kim, J.-W. Rhie, J.-H. Shim, D.-H. Kim, and D.-W. Cho, "Printing three-dimensional tissue analogues with decellularized extracellular matrix bioink.," *Nat. Commun.*, vol. 5, p. 3935, 2014.

[18] C. Frantz, K. M. Stewart, and V. M. Weaver, "The extracellular matrix at a glance.," *J. Cell Sci.*, vol. 123, pp. 4195–4200, 2010.

[19] A. Y. Belanger and A. J. McComas, "Contractile properties of human skeletal muscle in childhood and adolescence," *Eur J Appl Physiol Occup Physiol*, vol. 58, no. 6, pp. 563–567, 1989.

[20] D.-H. Kim, E. A. Lipke, P. Kim, R. Cheong, S. Thompson, M. Delannoy, K.-Y. Suh, L. Tung, and A. Levchenko, "Nanoscale cues regulate the structure and function of

macroscopic cardiac tissue constructs.," *Proc. Natl. Acad. Sci. U. S. A.*, vol. 107, no. 2, pp. 565–570, 2010.

[21] L. M. Larkin, S. Calve, T. Y. Kostrominova, and E. M. Arruda, "Structure and functional evaluation of tendon-skeletal muscle constructs engineered in vitro.," *Tissue Eng.*, vol. 12, no. 11, pp. 3149–58, 2006.

[22] H. S. Yang, N. Ieronimakis, J. H. Tsui, H. N. Kim, K. Y. Suh, M. Reyes, and D. H. Kim, "Nanopatterned muscle cell patches for enhanced myogenesis and dystrophin expression in a mouse model of muscular dystrophy," *Biomaterials*, vol. 35, no. 5, pp. 1478–1486, 2014.

[23] P. M. Gilbert, K. L. Havenstrite, K. E. G. Magnusson, A. Sacco, N. a Leonardi, P. Kraft, N. K. Nguyen, S. Thrun, M. P. Lutolf, and H. M. Blau, "Substrate elasticity regulates skeletal muscle stem cell self-renewal in culture. (Supplementary)," *Science*, vol. 329, no. 5995, pp. 1078–81, 2010.

[24] M. R. Lapin, J. M. Gonzalez, and S. E. Johnson, "Substrate elasticity affects bovine satellite cell activation kinetics in vitro," *J. Anim. Sci.*, vol. 91, no. 5, pp. 2083–2090, 2013.

[25] V. Gribova, C. Gauthier-Rouvière, C. Albigès-Rizo, R. Auzely-Velty, and C. Picart, "Effect of RGD functionalization and stiffness modulation of polyelectrolyte multilayer films on muscle cell differentiation," *Acta Biomater.*, vol. 9, no. 5, pp. 6468–6480, 2013.

[26] A. J. Engler, S. Sen, H. L. Sweeney, and D. E. Discher, "Matrix elasticity directs stem cell lineage specification.," *Cell*, vol. 126, no. 4, pp. 677–89, Aug. 2006.

[27] H. Vandenburgh, M. Del Tatto, J. Shansky, J. Lemaire, A. Chang, F. Payumo, P. Lee, A. Goodyear, and L. Raven, "Tissue-Engineered Skeletal Muscle Organoids for Reversible Gene Therapy," *Hum. Gene Ther.*, vol. 7, no. 17, pp. 2195–2200, Mar. 1996.

[28] S. V Murphy and A. Atala, "3D bioprinting of tissues and organs," *Nat. Biotechnol.*, vol. 32, no. 8, pp. 773–785, Aug. 2014.

[29] P. Mozetic, S. M. Giannitelli, M. Gori, M. Trombetta, and A. Rainer, "Engineering muscle cell alignment through 3D bioprinting," *Journal of Biomedical Materials Research - Part A*, 2017.

[30] J. Jang, H. J. Park, S. W. Kim, H. Kim, J. Y. Park, S. J. Na, H. J. Kim, M. N. Park, S. H. Choi, S. H. Park, S. W. Kim, S. M. Kwon, P. J. Kim, and D. W. Cho, "3D printed complex tissue construct using stem cell-laden decellularized extracellular matrix bioinks for cardiac repair," *Biomaterials*, vol. 112, pp. 264–274, 2017.

[31] T. L. Sellaro, A. Ranade, D. M. Faulk, G. P. McCabe, K. Dorko, S. F. Badylak, and S. C. Strom, “Maintenance of human hepatocyte function in vitro by liver-derived extracellular matrix gels.,” *Tissue Eng. Part A*, vol. 16, no. 3, pp. 1075–82, 2010.

[32] S. F. Badylak, D. O. Freytes, and T. W. Gilbert, “Extracellular matrix as a biological scaffold material: Structure and function,” *Acta Biomaterialia*, vol. 5, no. 1. pp. 1–13, 2009.

[33] M. T. Wolf, K. A. Daly, J. E. Reing, and S. F. Badylak, “Biologic scaffold composed of skeletal muscle extracellular matrix,” *Biomaterials*, vol. 33, no. 10, pp. 2916–2925, 2012.

[34] D. W. J. van der Schaft, A. C. C. van Spreeuwel, K. J. M. Boonen, M. L. P. Langelaan, C. V. C. Bouten, and F. P. T. Baaijens, “Engineering skeletal muscle tissues from murine myoblast progenitor cells and application of electrical stimulation.,” *J. Vis. Exp.*, no. 73, p. e4267, 2013.

[35] C. a Powell, B. L. Smiley, J. Mills, and H. H. Vandenburgh, “Mechanical stimulation improves tissue-engineered human skeletal muscle.,” *Am. J. Physiol. Cell Physiol.*, vol. 283, no. 5, pp. C1557–C1565, 2002.

[36] D. Seliktar, R. M. Nerem, and Z. S. Galis, “Mechanical strain-stimulated remodeling of tissue-engineered blood vessel constructs.,” *Tissue Eng.*, vol. 9, no. 4, pp. 657–666, 2003.

[37] M. Eastwood, V. C. Mudera, D. A. McGrouther, and R. A. Brown, “Effect of precise mechanical loading on fibroblast populated collagen lattices: Morphological changes,” *Cell Motil. Cytoskeleton*, vol. 40, no. 1, pp. 13–21, 1998.

[38] I. M. Bernstein, K. Plociennik, S. Stahle, G. J. Badger, and R. Secker-Walker, “Impact of maternal cigarette smoking on fetal growth and body composition.,” *Am. J. Obstet. Gynecol.*, vol. 183, no. 4, pp. 883–6, 2000.

[39] R. J. Goss, *Regulation of Organ and Tissue Growth.* Elsevier Science, 2013.

[40] H. Cho, H. Jönsson, K. Campbell, P. Melke, J. W. Williams, B. Jedynak, A. M. Stevens, A. Groisman, and A. Levchenko, “Self-organization in high-density bacterial colonies: Efficient crowd control,” *PLoS Biol.*, vol. 5, no. 11, pp. 2614–2623, 2007.

[41] J. Owens, K. Moreira, and G. Bain, “Characterization of primary human skeletal muscle cells from multiple commercial sources.,” *In Vitro Cell. Dev. Biol. Anim.*, vol. 49, no. 9, pp. 695–705, Oct. 2013.

VITA

Zeid Yousef Nawas was born and raised in Amman, Jordan. He earned a Bachelor's of Science in Bioengineering from the University of Washington in 2016. He earned a Master's of Science in Bioengineering from the University of Washington in 2017.